FRICTION MODELING AND EXPERIMENTAL IDENTIFICATION OF A MITSUBISHI PA10-6CE ROBOT MANIPULATOR

By

CHENG CHEN

A THESIS PRESENTED TO THE GRADUATE SCHOOL
OF THE UNIVERSITY OF FLORIDA IN PARTIAL FULFILLMENT
OF THE REQUIREMENTS FOR THE DEGREE OF
MASTER OF SCIENCE

UNIVERSITY OF FLORIDA

2013

To my parents for all their support to my graduate study and their encouragement which always inspires me to pursue academic goals

ACKNOWLEDGMENTS

I am foremost grateful to my advisor, Dr. Banks, who provided me with the opportunity to work in the Orthopaedic Biomechanics Laboratory, helped a lot with my research and taught me about how to live an academic life. I would like to thank Dr. Fregly for being my committee member and for many valuable suggestions. I also would like to thank my lab mates, Ira and Tim, for their great help in robotics and in how to become a qualified graduate student, and to thank Dr. Conrad for his arrangement in my experiment.

TABLE OF CONTENTS

LIST OF TABLES

LIST OF FIGURES

Abstract of Thesis Presented to the Graduate School
of the University of Florida in Partial Fulfillment of the
Requirements for the Degree of Master of Science

FRICTION MODELING AND EXPERIMENTAL IDENTIFICATION OF A MITSUBISHI PA10-6CE ROBOT MANIPULATOR

By

Cheng Chen

May 2013

Chair: Scott Banks
Major: Mechanical Engineering

The purpose of this paper is to evaluate the effects of extra loads, different velocity ranges and different friction models on friction parameter identification of a PA10-6CE robot manipulator. A reformulated rigid-link flexible-joint dynamic model including the friction function is applied to identify the friction parameters of a robot with harmonic drive joint transmissions. Motion capture is used to measure the link position as an additional experimental tool. Finite Fourier series and optimization methods are used in trajectory design and friction parameter fitting to provide a well conditioned computational system. A Coulomb plus viscous model, a four-parameter Stribeck model and a continuous hyperbolic model are implemented as friction models, and parameter estimation robustness is compared. The reliability, repeatability and applicability of each model are analyzed based upon the experimental data.

CHAPTER 1
INTRODUCTION

Dynamic modeling with accurate experimental parameter identification is essential to improve the performance of robot control and realistic simulation. Velocity dependent friction is regarded as one of the most complicated terms in robot dynamic modeling since it can vary dramatically over different velocity ranges. Although precise and reliable friction identification experiments for rigid joint robots have been well reported (Khosla, 1985 and Johnson, 1992), methods and results for robots with flexible joints, such as the Mitsubishi PA10-6CE with harmonic drive transmissions, are less well established or generally used.

Based on considerations of tribology and related physics, Armstrong *et al.* (1991) surveyed friction compensation control strategies for robotics. The conventional Coulomb plus viscous friction model was compared to a Stribeck friction model that included a negative viscous period before Coulomb friction. Armstrong *et al.* developed a seven parameter integrated friction model with Stribeck effects based upon their review of previous work. Several related studies have been conducted to identify friction properties in mechanisms and to verify the Stribeck phenomenon with various models. Tuttle (1992) implemented a cubic polynomial to approximate friction in harmonic drives and found a linear relationship between friction and velocity. Taghirad (1997) investigated friction in harmonic drives and described a Stribeck friction formulation using simulation and experimental results. Canudas *et al.* (1995) created a bristle-based dynamic friction model containing the Stribeck effect, hysteresis and spring-like properties. This model was subsequently adopted and modified by Swevers (2000). In order to fulfill the requirements of high-performance controllers, a continuously

differentiable friction model was proposed by Makkar *et al.* (2005) with six hyperbolic terms. Simultaneously exhibiting Coulomb, viscous, static and Stribeck effects, Makkar's model was verified in a numerical simulation.

Friction in harmonic drives mounted in robot manipulators is not solely a function of joint velocity, so a practical model must account for other factors including assembly, load, and bearing preload. Thus, friction modeling and robot parameter identification require different approaches since removal of the harmonic drive from a robot is impractical and changes friction characteristics of real working conditions. Kennedy *et al.* (2003) determined the friction-velocity relationship for each joint in a PA-10 robot by moving single joints at a constant velocity and recording the mean torque required to maintain this motion. A four-parameter friction model was implemented to express Stribeck, Coulomb and viscous properties. Bompos *et al.* (2007) carried out similar constant velocity experiments with a six-parameter friction model. In their experiments, the link position was measured from the resolver in each joint. Lightcap *et al.* (2007) used motion capture and optimized trajectories to identify all dynamic parameters of a PA10-6CE robot, one joint at a time, using Coulomb and viscous terms for friction.

One objective of this paper is to compare the consistency, robustness and reliability of three different friction models for a range of experimental conditions. Kennedy *et al.* (2003) made a comparison between viscous, cubic and Stribeck friction models at a single joint velocity of 0.4 rad/s. Bompos and Lightcap identified the friction parameters under conditions where the maximum joint velocity was about half the velocity limit for that joint. However, there is both practical and theoretical interest to study robot dynamics, particularly friction, over the entire velocity range.

Trajectory optimization for system identification is another significant technical issue for appropriate experiment design and robustness of model parameters. Swevers *et al.* (1996) designed periodic trajectories by minimizing the condition number of a regressor matrix which reduced the effects of measurement noise and improved parameter identification accuracy. Finite Fourier series were used to parameterize trajectories and the Fourier coefficients were treated as design variables in the optimization. Calafiore *et al.* (2001) developed an optimal trajectory design method which minimized the logarithmic determinant of the Fisher information matrix and was carried out on a two-link planar manipulator. Since small position residue was achieved in their experiments, finite Fourier series were also implemented to calculate joint velocity and acceleration.

This paper applies a rigid-link flexible-joint robot dynamic parameter identification method to evaluate the effects from external loads, velocity ranges and different friction models on parameter identification. Section 2 introduces three different types of friction models and reformulates the dynamic equation of a one-link robot manipulator. Section 3 describes the computational methods for trajectory design and joint angle calculation from motion capture data. Section 4 discusses the experimental process. In section 5 and 6, the experiment data is analyzed and discussed, and conclusions are drawn from the comparison between each friction model.

CHAPTER 2
MODELING

Rigid-Link Flexible-Joint Model

The motor position and the link position of the PA-10 robot arm should be parameterized separately in order to exhibit the joint flexibility of the robot manipulator. Then the dynamics of an n-link rigid-link flexible-joint (RLFJ) can be modeled as (Spong, 1987):

$$M(q)\ddot{q} + V_m(q,\dot{q})\dot{q} + G(q) + F(\dot{q}) + K(q - q_m) = 0$$

$$J\ddot{q}_m + B\dot{q}_m + K(q_m - q) = u \tag{2-1}$$

where $q(t), \dot{q}(t), \ddot{q}(t) \in \Re^{\mathrm{n}}$ and $q_m(t), \dot{q}_m(t), \ddot{q}_m(t) \in \Re^{\mathrm{n}}$ express the joint position, velocity and acceleration of the link and motor angle, respectively, $M(q) \in \Re^{\mathrm{n}\times\mathrm{n}}$, $V_m(q,\dot{q}) \in \Re^{\mathrm{n}\times\mathrm{n}}$, $G(q) \in \Re^{\mathrm{n}}$ and $F(\dot{q}) \in \Re^{\mathrm{n}}$ represent the inertia matrix, the centripetal-Coriolis matrix, gravitational and frictional effects of the link dynamics respectively, $K, B, J \in \Re^{\mathrm{n}}$ denote the joint stiffness, motor viscous friction and motor inertia which are all constant, diagonal, positive-definite matrices. To simplify the calculation of the dynamic equation, the gear ratio is included in the expression of the motor position.

The dynamic model of a one-link RLFJ robot can be expressed as:

$$I\ddot{q} - mgl_x \sin(q) + mgl_y \cos(q) + f(\dot{q}) + k(q - q_m) = 0$$

$$J\ddot{q}_m + B\dot{q}_m + k(q_m - q) = u \tag{2-2}$$

where $q(t), \dot{q}(t), \ddot{q}(t) \in \Re^{\mathrm{n}}$ and $q_m(t), \dot{q}_m(t), \ddot{q}_m(t) \in \Re^{\mathrm{n}}$ are measurable parameters in the experiment representing the joint position, velocity and acceleration of the link and motor angle respectively, $I, m \in \Re$ denote the link inertia and mass respectively, $J, B \in \Re$ are the motor inertia and viscous friction which can be obtained from the

manufacturer or previous experiments (Lightcap, 2007), and $f(\dot{q})$ represents the frictional term to be modeled.

As weak robot joint elasticity (i.e. stiff joints) leads to poorly scaled equations for computation, the stiffness term is substituted from Equation 2-2. Therefore, the one-link dynamic equation can be rewritten as:

$$I\ddot{q} - mgl_x \sin(q) + mgl_y \cos(q) + f(\dot{q}) + J\ddot{q}_m + B\dot{q}_m = u \quad (2\text{-}3)$$

However, this scenario still requires very high experimental accuracy and computational sensitivity to separate the link inertia and viscous coefficients and those of the motor since the deflections are small. Previously measured motor inertia and viscous friction parameters can be used in the calculation to enhance the robustness of the optimization and the dynamic equation can be reformulated as:

$$I\ddot{q} - mgl_x \sin(q) + mgl_y \cos(q) + f(\dot{q}) = u - J\ddot{q}_m - B\dot{q}_m \quad (2\text{-}4)$$

Now the frictional, gravitational and inertial terms in a one-link model of the robot manipulator can be identified with a better conditioned numerical system. Link positions (q's) are measured using a motion capture system, and linear or nonlinear optimization is used to solve for parameters in an overdetermined system of experimental data.

Frictional Models

Coulomb + Viscous model. Velocity dependent Coulomb friction and viscous friction with simple mathematical expressions are two basic factors in frictional models. This simple model can be written as:

$$f(\dot{q}) = c\ sign(\dot{q}) + v\ \dot{q} \quad (2\text{-}5)$$

Accordingly, the friction force is linearly dependent on velocity with a constant Coulomb value based on the direction of motion.

Substituting Equation 2-5 into Equation 2-4, we have the regressor matrix:

$$R = [\ddot{q} \quad -\sin(q) \quad \cos(q) \quad sign(\dot{q}) \quad \dot{q}\ ] .$$

Least-squares methods are applied to solve this model and this matrix can be implemented to optimize the manipulator trajectory in the experiment to improve computational robustness.

Four-parameter Stribeck model. A four-parameter Stribeck model can be used to capture the negative viscous friction phenomenon at low velocities:

$$f(\dot{q}) = F_k\ sign(\dot{q}) + F_v\ \dot{q} - sign(\dot{q})\ F_s(1 - e^{\left(-\frac{sign(\dot{q})\ \dot{q}}{V_c}\right)}) \tag{2-6}$$

where F_k and F_v denote the Coulomb and viscous friction coefficients, respectively, and $F_s(1 - e^{\left(-\frac{sign(\dot{q})\ \dot{q}}{V_c}\right)})$ represents the Stribeck effect of negative viscous friction at low velocities. Nonlinear optimization methods in MATLAB (Mathworks, Natick, MA) are utilized to fit overdetermined data sets to this model.

Hyperbolic model. A continuously differentiable friction model for high-performance controllers can be expressed as the combination of hyperbolic terms (Makkar, 2005). With six parameters, the hyperbolic friction model can present comprehensive velocity dependent frictional characteristics based upon a nonlinear symmetric form. Friction force is expressed as:

$$f(\dot{q}) = \gamma_1(\tanh(\gamma_2\dot{q}) - \tanh(\gamma_3\dot{q})) + \gamma_4 \tanh(\gamma_5\dot{q}) + \gamma_6\dot{q} \tag{2-7}$$

where the Coulomb and viscous dissipation friction are denoted by the terms $\gamma_4 \tanh(\gamma_5\dot{q})$ and $\gamma_6\dot{q}$, respectively, the static coefficient of friction is assumed to be approximated by $\gamma_1 + \gamma_4$, and the Stribeck effect at low velocity is represented by $\tanh(\gamma_2\dot{q}) - \tanh(\gamma_3\dot{q})$.

Similar to the four-parameter Stribeck friction model, the six design variables in this hyperbolic model are also fitted by nonlinear optimization with an initial guess from the Coulomb + Viscous model.

CHAPTER 3
METHODS

Finite Fourier Series and Trajectory Design

It has been shown that a well designed trajectory can sufficiently excite the dynamics and frictional properties of a rigid-link flexible-joint robot. Finite Fourier series are commonly used to approximate periodic trajectories with all the harmonics as design variables in the optimization. Therefore, the optimization criteria can be selected to minimize the condition number of the regressor matrix (Swevers, 1996). The purpose of using finite Fourier series approximations for trajectory optimization is to enhance the computational robustness and improve the reliability and accuracy of velocity and acceleration calculations. Thus, the nonlinear optimization with linear constraints can be expressed as:

$$\min cond(R)$$

$$s.t \begin{cases} |q(t)| < q_{limit} \\ |\dot{q}(t)| < \dot{q}_{limit} \\ |\ddot{q}(t)| < \ddot{q}_{limit} \end{cases} \tag{3-1}$$

where the link position constituting the regressor matrix is approximated by the motor position (a rigid joint approximation), and the position and velocity limits are provided by the robot manufacturer. Based on finite Fourier series, the link position, velocity and acceleration can be given as:

$$\begin{aligned} q(t) &= \sum_{l=1}^{N} \frac{a_l}{w_f l} \sin(w_f lt) - \frac{b_l}{w_f l} \cos\left(w_f lt\right) + q_0 \\ \dot{q}(t) &= \sum_{l=1}^{N} a_l \cos(w_f lt) + b_l \sin(w_f lt) \\ \ddot{q}(t) &= \sum_{l=1}^{N} a_l w_f l \, sin(w_f lt) + b_l w_f l \cos\left(w_f lt\right) \end{aligned} \tag{3-2}$$

where w_f represents the fundamental frequency, chosen as the natural frequency of the robot, and a_l and b_l denote amplitudes of harmonics as design variables. Different velocity ranges are used to assess friction model parameters from different conditions, thus peak velocities corresponding to 100%, 50% and 25% of the manufacturer specified maximum joint velocity are used for separate tests. Zero initial and final velocity and acceleration conditions are design constraints to ensure safe and realizable trajectories.

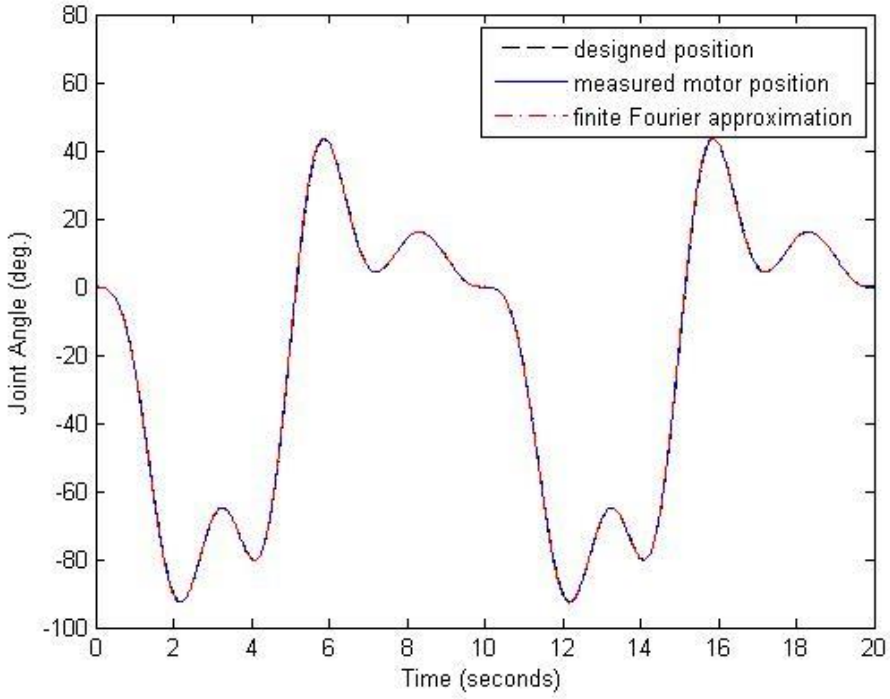

Figure 3-1. The designed, measured, and approximated trajectories for Link 3.

If the control system is properly designed, the robot arm will exhibit relatively good trajectory tracking behavior, and the finite Fourier series approximation can also be applied to fit the experimental data to the link and motor positions. Figure 3-1 shows the optimization result of the designed trajectory and the experimental results for joint and link 3. The data indicate the feed-forward controller used in the experiment has

small tracking errors for well-designed trajectories, and that finite Fourier series can provide excellent approximations with average errors less than 0.05 degree. The motor velocity and acceleration can then be calculated according to the finite Fourier approximation shown in Figure 3-2. Similarly, the link velocity and acceleration can also be computed through this method.

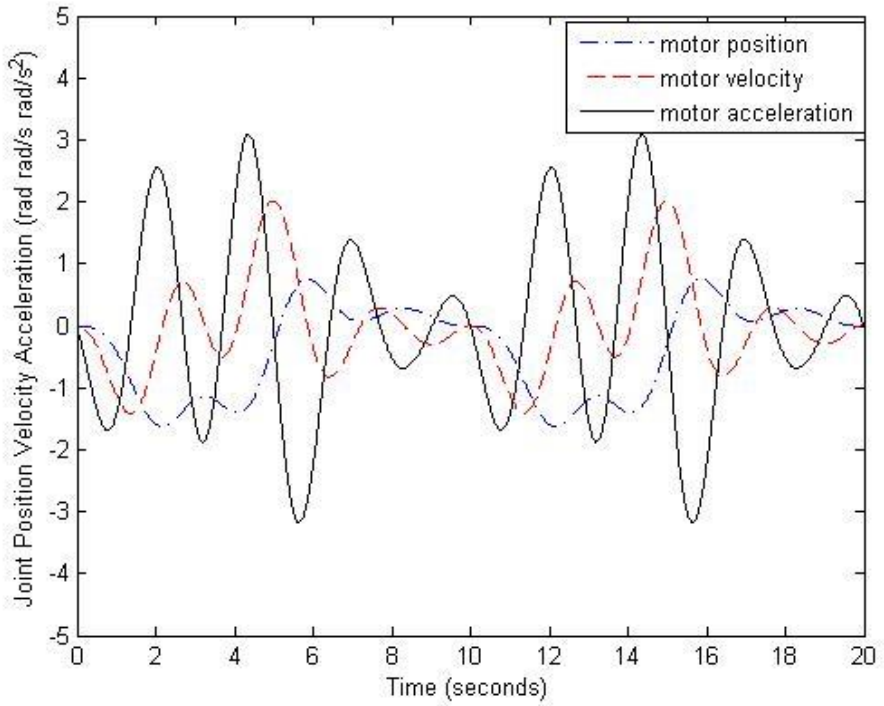

Figure 3-2. The joint position, velocity and acceleration from finite Fourier approximations for Link 3.

Estimation of Link Position

Although the PA10-6CE robot manipulator is assembled with two encoders on both sides of the harmonic drive in each joint, we only have access to the data from the motor side encoder. Therefore, the link position needs to be measured by the motion capture system due to joint flexibility. Figure 3-3 shows that motion capture markers are attached on the surface of the robot.

To calculate the link position, we first have to know the relative position of the robot to the camera system, in other words, the transformation matrix from the cameras to the fixed base of the robot ${}^{c}_{f}T$. The unit vector of an axis of rotation, and the coordinate of one point on that axis, can be computed by rotating a single joint around a fixed axis (Halvorsen, 2003). The relative position of the robot to the camera system can be determined by individually rotating joints one and two and calculating the intersection of these two axes of rotation in the camera reference system.

In a rigid link robot arm, the coordinates of each reflective marker evaluated in its corresponding link coordinate system is constant in every data frame. Implementing coordinate transformations, we have:

$$ {}^{n}P_{m}^{p} = {}^{n}_{c}T^{p} \times {}^{c}P_{m}^{p} \tag{3-3} $$

where ${}^{n}P_{m}^{p}$ is the position of marker m measured in the coordinate system fixed in link n in frame p , ${}^{c}P_{m}^{p}$ is the position of that marker measured in the motion capture system in frame p and ${}^{n}_{c}T^{p}$ denotes the transformation matrix from the coordinate system fixed in link n to the cameras in frame p. With all the constant geometric parameters of the robot from the manufacturer, the only unknown and time-varying parameters in the transformation matrix are the link angles. Furthermore, the left hand side of the Equation 3-3 is constant in every frame since marker m is fixed on that link.

To approximate the relative position of each marker corresponding to the coordinate system of its fixed link, a static pose is applied. In that frame, the robot doesn't move and joint flexibility can be ignored. Therefore, the joint angles of the link can be obtained directly from the joint encoder. Then the relative position of the marker in a static pose can be calculated as:

$$ {}^{n}P_{m}^{static} = {}_{c}^{n}T^{static} \times {}^{c}P_{m}^{static} \tag{3-4} $$

After the static position of each marker corresponding to its fixed link is computed, a nonlinear optimization can be built to obtain the link position. The cost function of link n in frame p is defined as:

$$ E = \min \sum_{m=1}^{m} ({}^{n}P_{m}^{p} - {}^{n}P_{m}^{static})^{2} \tag{3-5} $$

where ${}^{n}P_{m}^{p}$ is calculated by using the transformation matrix from the motion capture system to link n and the measured position of marker m in the camera's in frame p. In this case, m markers are utilized to construct an overdetermined optimization and the motor position is chosen as the initial guess.

This method can also be used to calculate the link position in the situation where multiple links of a robot are simultaneously moving. As discussed above, the only design variable of the optimization is the joint angle and the computation is carried out in a single frame. However, more design variables, such as the geometric parameters, can be applied and more frames can be simultaneously used in the optimization of this method.

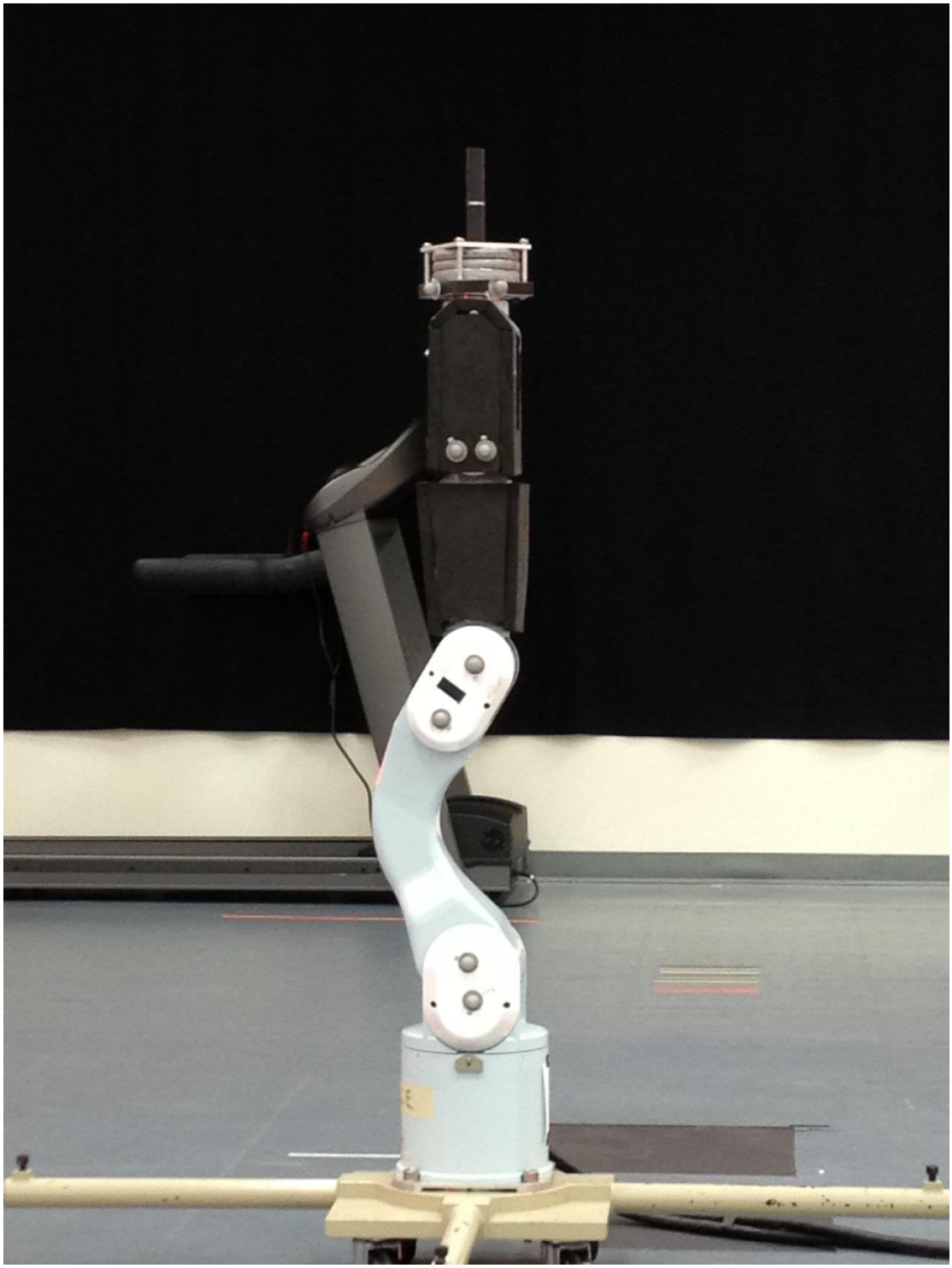

Figure 3-3. Motion capture markers fixed on the surface of PA10-6CE. (Photo courtesy of author)

CHAPTER 4
EXPERIMENT

Figure 4-1 shows the setup of the experiment where a PA10-4CE robot manipulator was mounted on a floor stand and placed in the center of the viewing volume of a twelve-camera motion capture system (Motion Analysis Corporation, Santa Rosa, CA). Sixteen passive reflective markers were attached on the exterior surface of the robot links. The motion capture system was calibrated and the 3D residual measurement error was recorded as 0.845 mm (S.D. 0.21 mm). A real-time computer, CompactRio (National Instruments Corporation, Austin, TX), was used to control the robot and collect measurement data. Synchronized data with time stamps from the robot and the motion capture system were streamed to a host computer at a frequency of 200Hz.

The experiment was conducted in two groups of trials. A 33.075 N load was mounted on the robot end-effector for one group of trials and the second group of trials had no additional end-effector load. The optimized single-joint trajectories were followed for each individual robot joint and repeated for each group of trials. Electro-magnetic brakes were used for inactive links. Three different velocity boundaries were designed for each joint with the highest maximum velocity in one trajectory being the velocity limit of that joint and the lowest velocity boundary being 10% of the limit. Each trajectory was repeated five times to establish repeatability.

During the experiment, the motor position was measured by the joint encoders with a resolution of 0.011 degree for the angular position. The motor torque was computed from the input motor current and motor torque constant. The link position was calculated offline by using the marker position data from the motion capture system.

Finite Fourier series were used to fit the link position to a continuous function in order to synchronize the link and motor position. Friction models were fit to the experimental data using linear or nonlinear optimization. The sample mean value and a coefficient of variation (CV) for each friction parameter were calculated as experiment results.

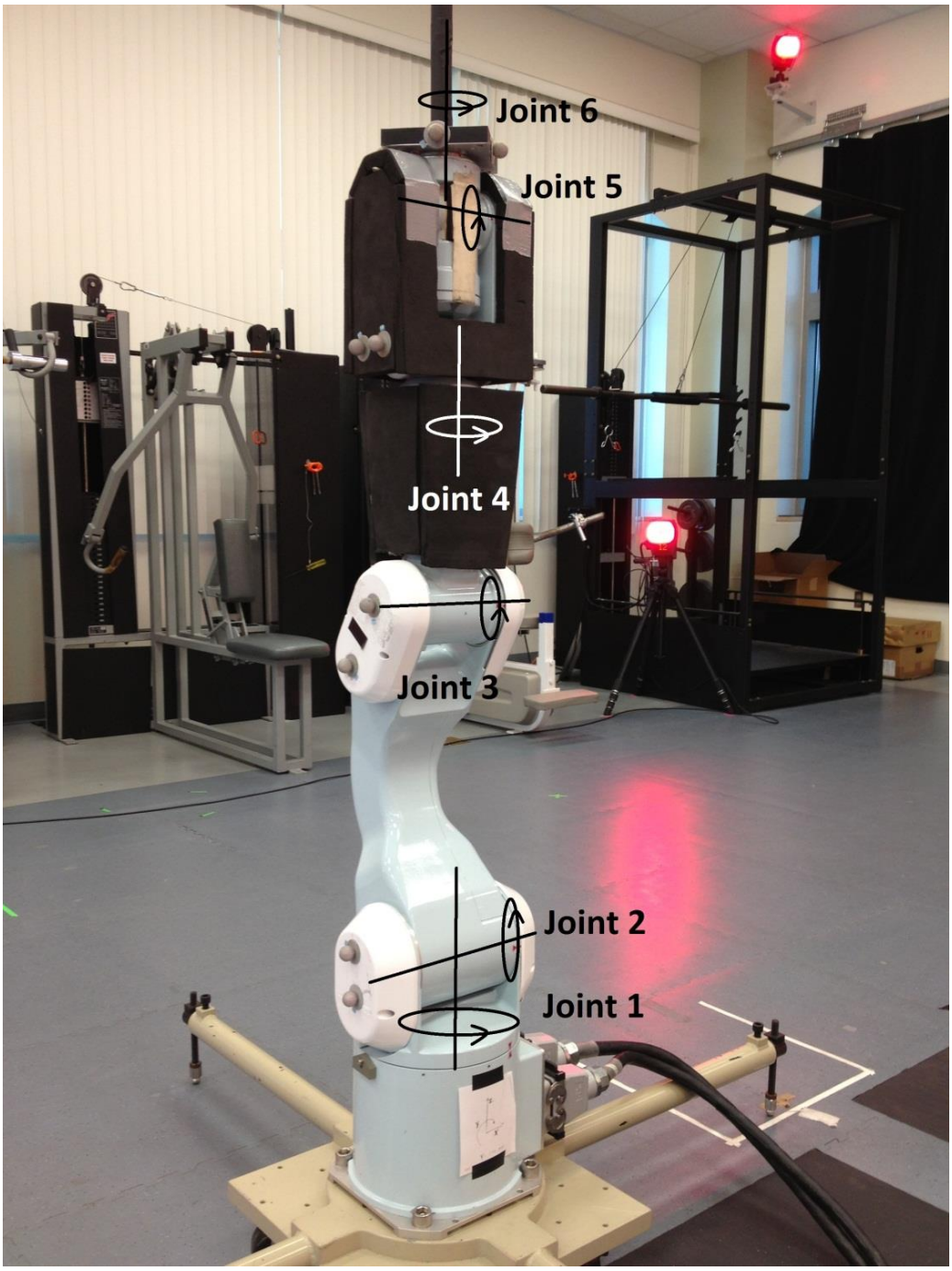

Figure 4-1. Configuration of the robot in the experiment. (Photo courtesy of author)

CHAPTER 5
RESULT AND DISCUSSION

The velocity dependent friction parameters for three friction models are reported in Table 5-1. The root mean square (RMS) error in the estimation of the friction torque and its percentage of the maximum motor torque for joints 4 and 5 are shown in Table 5-2. The results of the remaining joints are reported in the Appendix. Most CV values for Coulomb friction terms, and RMS errors in the Coulomb plus viscous model, were below 10% and indicate consistent data was obtained from repeated trials. The percentages of the RMS error, proportional to the motor torque of that joint, were less than 9% of maximum motor torque in that trial. In terms of finite Fourier approximation, the computational error was less than 0.05 degree for motor angles and 0.2 degree for link positions.

Both experimental and computational sources of error were produced in the identification process. With the calibration error from the motion capture system, the optimization for estimating the link position had a residual error of marker position of approximate 0.9 mm in each joint. The measured input torque computed from the current did not include the variability of motor constant and the efficiency of gear transmission in different assembly and working conditions. The inaccuracy of the geometric parameters of the robot from the manufacturer and the motor inertia and viscous parameters from previous studies (Lightcap, 2007 and Lightcap, 2008) contributed additional uncertainties to the optimization. In terms of friction, the sensitivity of joint angle measurement caused difficulty in modeling static friction, and position dependent friction (Tuttle, 1992) was not included in the models. In addition, single-link

trajectories reduced the accuracy of the experiment since joints locked by electro-magnetic brakes may still deflect slightly under load.

Based on the experimental results, several factors influencing friction parameter estimation are identified.

Extra End-Effector Load

Extra end-effector load has been claimed to influence friction parameters (Armstrong, 1991) and to better excite robot dynamics for better parameter estimation (Lightcap, 2008). By comparing the experimental results of the loaded (33.1 N) and unloaded groups, the following conclusions can be drawn:

- There was no obvious change in either Coulomb or viscous friction terms for any of the three friction models with extra end-effector load.
- The extra-load group estimates showed more consistent parameters with smaller CV values and better model fits with smaller RMS errors, especially for joints 4, 5 and 6.

Velocity Ranges

For each joint, three different trajectories were designed with velocity boundaries ranging from 100% to about 20% of the maximum joint velocity. Friction models were fit based upon the data from each trajectory, and several conclusions can be drawn from the data shown in Table 5-1 and the Appendix.

- The Coulomb friction coefficient for all three friction models was not significantly affected by experiment velocity ranges. This indicates that Coulomb friction remains constant and does not change measurably as the velocity magnitude is varied.
- As the velocity boundary increased, the viscous term decreased. Figure 5-1 shows an example of the effect of experimental velocity range on friction parameters for joint 5.
- The CV for each model parameter was higher for low velocity conditions since friction torques are smaller, the signal-to-noise ratio is smaller, and the sensitivity for parameter estimation is reduced.

- RMS errors reached their lowest values for medium velocity trajectories in some joints. This may be due to other mechanical factors, such as soft wind-up and friction hysteresis at low velocities, and model applicability across the whole robot velocity range.

Different Friction Models

It is essential to verify the reliability and accuracy of different friction models in the PA10 robot. According to the experimental data and analysis, the hyperbolic friction model with six parameters obtained the lowest RMS errors among the three models. It is obvious to conclude that greater degrees of freedom in the friction model contributes to lower model-fitting error. On the other hand, the Coulomb plus viscous friction model exhibited the best parameter repeatability, with the smallest CV in all the joints. An example of a comparison among three friction models is shown in Figure 5-2.

The Coulomb plus viscous friction model captures the basic frictional properties of the PA10 robot. The two most significant friction parameters were conveniently fitted with good convergence during a number of trials. However, relatively large RMS residual errors remain, and the negative viscous friction phenomenon at low velocities cannot be captured by this simple model.

A four-term Stribeck model was utilized to enhance the ability to capture low-velocity friction properties, which involved adding two terms, F_s and V_c, to the Coulomb plus viscous friction model. Smaller RMS errors were achieved, and negative viscous friction at low joint velocities was approximated. However, due to the similarity with the Coulomb plus viscous friction model, the four-parameter Stribeck model could converge to two entirely different forms: The first form had F_s very close to 0, and the model degenerated to the Coulomb plus viscous model (joint 3). In the second form (joint 5), F_k was approximately 0 with a small V_c and the Coulomb friction was expressed by a

negative F_s. Therefore, very large CV values for fitting F_s and F_k resulted without extremely high measurement sensitivity and properly designed optimization parameter boundaries. Furthermore, Stribeck effect can only be represented by a positive F_s and a small V_c value for normal mechanisms.

In the six-parameter hyperbolic model γ_4 and γ_6, which denote the Coulomb and viscous friction coefficients, had the best repeatability during the repeated trials. The values of the remaining design parameters varied dramatically across trials even though the negative viscous friction phenomenon was clearly shown. This indicated that non-unique combinations of γ_1, γ_2 and γ_3 can lead to similar overall values for the expression of the Stribeck effect using this model. The static friction term, claimed to be represented as $\gamma_1 + \gamma_4$, could not be properly modeled since high enough experimental accuracy could not be obtained.

Table 5-1. Friction parameter identification results of Coulomb plus viscous and Stribeck model for joint 5.

Joint	Extra load (N)	Maximum velocity (rad/s)	Statistic	Coulomb + viscous model		Four-parameter Stribeck model			
				c	v	F_k	F_v	F_s	V_c
5	33.1	2.43	mean	4.13	1.17	<0.01	1.01	-4.63	<0.01
			CV(%)	3.10	2.73	n/a	2.99	2.88	n/a
		1.58	mean	3.88	1.56	<0.01	1.38	-4.16	<0.01
			CV(%)	0.57	1.05	n/a	1.17	0.55	n/a
		0.80	mean	3.62	2.57	0.79	1.76	3.56	<0.01
			CV(%)	1.32	2.49	200.00	20.27	54.66	n/a
	0	2.42	mean	3.90	0.84	<0.01	0.67	-4.41	<0.01
			CV(%)	2.67	4.46	n/a	3.45	0.88	n/a
		1.58	mean	3.89	1.37	0.53	1.14	-3.70	0.01
			CV(%)	1.63	1.64	80.39	2.05	10.28	18.58
		0.79	mean	3.62	2.66	0.80	1.83	-3.58	0.01
			CV(%)	2.70	12.36	200.00	40.28	57.15	50.22

Table 5-2. Friction parameter identification results of hyperbolic model for joint 5.

Joint	Extra load (N)	Maximum velocity (rad/s)	Statistic	Six-parameter hyperbolic model					
				γ_1	γ_2	γ_3	γ_4	γ_5	γ_6
5	33.1	2.43	mean	5.02	161.40	5.37	5.01	4.18	0.81
			CV(%)	7.11	9.31	11.83	2.47	6.54	4.88
		1.58	mean	6.49	105.85	30.43	4.44	19.37	1.22
			CV(%)	2.09	2.46	1.43	0.44	1.26	1.30
		0.80	mean	27.63	88.87	22.16	4.56	18.88	1.53
			CV(%)	163.20	17.07	91.72	3.95	80.26	14.07
	0	2.42	mean	4.70	157.77	4.82	4.87	3.77	0.42
			CV(%)	0.67	16.19	5.21	2.70	5.33	10.34
		1.58	mean	106.10	52.50	49.12	4.57	20.29	0.93
			CV(%)	26.07	4.22	2.15	1.70	3.03	1.06
		0.79	mean	84.21	72.12	49.87	4.40	36.66	1.85
			CV(%)	51.53	26.82	40.87	6.94	35.88	33.80

Table 5-3. Root mean square error of three different friction models for joint 4 and joint 5.

Joint	Extra load (N)	Maximum velocity (rad/s)	RMS error	Coulomb + viscous model	Stribeck model	Hyperbolic model
4	33.1	2.00	mean(Nm)	0.27	0.19	0.19
			CV(%)	3.57	5.69	5.78
			percentage(%)	5.48	3.89	3.80
		1.51	mean(Nm)	0.18	0.17	0.17
			CV(%)	4.83	4.89	4.91
			percentage(%)	3.90	3.73	3.67
		0.81	mean(Nm)	0.17	0.12	0.12
			CV(%)	12.34	25.11	27.08
			percentage(%)	3.96	2.89	2.80
	0	2.00	mean(Nm)	0.32	0.25	0.24
			CV(%)	6.18	10.97	11.65
			percentage(%)	5.70	4.44	4.36
		1.51	mean(Nm)	0.23	0.20	0.19
			CV(%)	0.41	0.51	0.52
			percentage(%)	4.41	3.88	3.78
		0.79	mean(Nm)	0.35	0.26	0.25
			CV(%)	51.68	82.61	85.56
			percentage(%)	6.37	4.78	4.66
5	33.1	2.43	mean(Nm)	0.83	0.61	0.58
			CV(%)	8.72	12.88	12.25
			percentage(%)	7.16	5.22	2.01
		1.58	mean(Nm)	0.58	0.47	0.45
			CV(%)	1.81	1.68	1.77
			percentage(%)	4.69	3.79	3.63
		0.80	mean(Nm)	0.66	0.53	0.49
			CV(%)	3.55	9.63	3.04
			percentage(%)	7.27	5.85	5.41
	0	2.42	mean(Nm)	0.80	0.57	0.54
			CV(%)	3.55	9.63	3.04
			percentage(%)	7.27	5.85	5.41
		1.58	mean(Nm)	0.64	0.55	0.53
			CV(%)	1.82	4.49	5.41
			percentage(%)	6.66	5.72	5.53
		0.79	mean(Nm)	0.67	0.53	0.50
			CV(%)	7.40	22.45	16.03
			percentage(%)	8.38	6.63	6.24

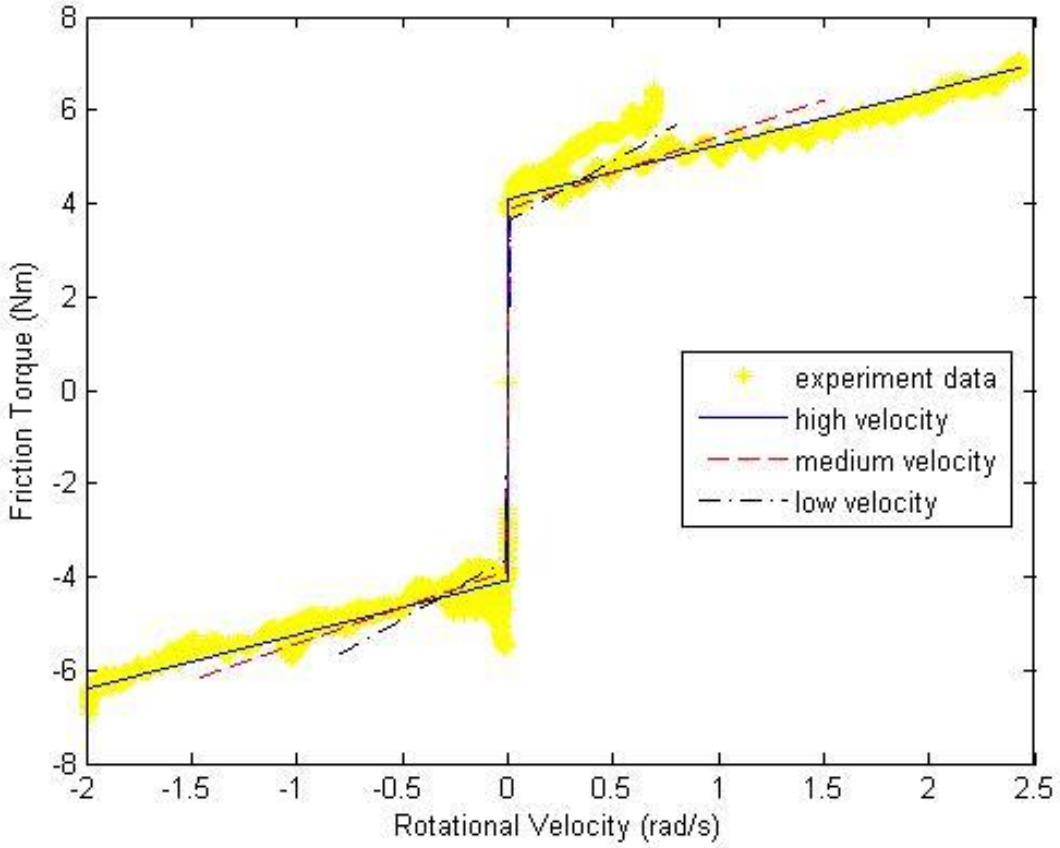

Figure 5-1. Experimental data and fitted Coulomb plus viscous friction model for three different velocity ranges for joint 5.

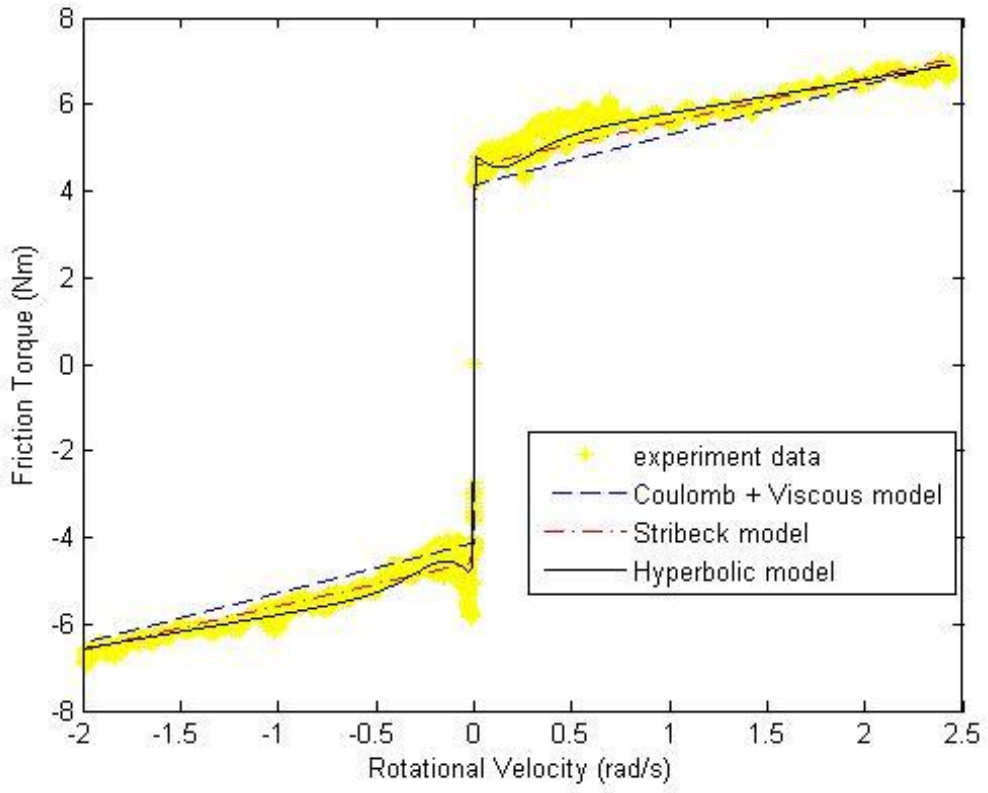

Figure 5-2. Experimental data compared to three friction models in high velocity range for joint 5.

CHAPTER 6
CONCLUSIONS

In this paper we have presented our approach for identifying friction parameters in three different models through experiments with a RLFJ robot manipulator. We first established the dynamic model of the robot including the friction function which took the joint flexibility of harmonic drives into account. A motion capture system was used to measure the link position as an additional tool of the experiment. Linear and nonlinear optimization methods were applied to solve for friction parameters of each model and comparison was made among different friction models based on the experimental data. The reliability and repeatability of each friction model were analyzed at different velocity ranges.

Compared to the dynamic model of rigid joint robot, the model involving joint flexibility is more accurate and practical to describe the robot arm installed with harmonic drives. With the development of precise cameras and real-time data transmission, motion capture systems can contribute significantly in research of robotics and human-robot interaction. The experimental method discussed in this paper has the advantage over the constant velocity method (Kennedy, 2003) since it includes gravitational terms in the dynamic model which reduce inaccuracy when installing the robot arm in typical standing configurations.

Different friction models have their corresponding applicable velocity ranges. For example, the four-parameter Stribeck model can capture the negative viscous friction in low velocity, but tends to degenerate to Coulomb plus viscous model in relatively high velocity. Therefore, it is crucial to use the friction model in control loops based on the working velocity to achieve high accuracy.

Further efforts will be focused on two main areas. One is to improve the accuracy of dynamic identification and design multi-link trajectories for more practical working conditions. The other is to apply the identified friction model to the control strategy (Dixon, 2000) and to achieve better model-based tracking performance.

APPENDIX A
FRICTION PARAMETER IDENTIFICATION RESULTS

Table A-1. Friction parameter identification results of Coulomb plus viscous and Stribeck model for joint 1.

Joint	Extra load (N)	Maximum velocity (rad/s)	Statistic	Coulomb + viscous model		Four-parameter Stribeck model			
				c	v	F_k	F_v	F_s	V_c
1	33.1	1.00	mean	9.86	5.47	0.04	4.24	-11.06	0.01
			CV(%)	0.51	4.55	200.00	4.46	1.31	7.92
		0.50	mean	8.44	12.52	<0.01	7.72	-10.91	0.01
			CV(%)	1.77	0.84	n/a	1.88	1.53	2.39
		0.34	mean	8.87	15.30	1.02	8.12	-10.37	0.01
			CV(%)	1.15	1.72	200.00	13.74	23.51	16.94
	0	1.00	mean	9.53	5.62	<0.01	4.37	-10.81	0.01
			CV(%)	1.01	2.70	n/a	3.27	1.44	4.18
		0.50	mean	8.68	12.09	<0.01	7.37	-11.09	0.01
			CV(%)	2.66	1.70	n/a	3.36	2.05	1.77
		0.34	mean	10.05	19.31	<0.01	10.12	-13.27	0.01
			CV(%)	9.14	9.06	n/a	9.70	9.77	1.21

Table A-2. Friction parameter identification results of hyperbolic model for joint 1.

Joint	Extra load (N)	Maximum velocity (rad/s)	Statistic	Six-parameter hyperbolic model					
				γ_1	γ_2	γ_3	γ_4	γ_5	γ_6
1	33.1	1.00	mean	13.62	95.24	14.38	11.30	10.62	3.84
			CV(%)	2.71	8.81	5.09	0.83	6.67	5.99
		0.50	mean	261.40	62.75	59.48	10.61	39.75	8.42
			CV(%)	13.06	3.34	2.68	1.59	3.82	1.77
		0.34	mean	157.70	76.34	70.69	10.99	61.71	9.55
			CV(%)	19.53	1.78	2.48	1.25	6.04	3.87
	0	1.00	mean	14.01	86.94	16.13	10.92	11.98	4.12
			CV(%)	3.54	4.27	9.34	1.71	9.26	3.65
		0.50	mean	250.10	59.11	55.62	10.87	34.55	7.90
			CV(%)	19.61	3.08	2.85	2.22	3.94	2.35
		0.34	mean	199.50	75.39	70.26	12.56	60.95	12.47
			CV(%)	25.09	0.93	0.57	9.97	4.93	9.17

Table A-3. Friction parameter identification results of Coulomb plus viscous and Stribeck model for joint 2.

Joint	Extra load (N)	Maximum velocity (rad/s)	Statistic	Coulomb + viscous model		Four-parameter Stribeck model			
				c	v	F_k	F_v	F_s	V_c
		1.01	mean	12.44	26.96	2.00	23.82	-14.39	0.00
			CV(%)	14.87	3.25	200.00	0.53	22.22	66.15
	33.1	0.51	mean	12.69	39.07	12.76	83.87	57.16	1.00
			CV(%)	2.16	1.91	2.15	8.34	15.52	0.00
		0.26	mean	4.41	79.81	4.45	435.29	401.90	1.00
2			CV(%)	44.02	8.56	32.55	16.50	18.57	0.00
		1.01	mean	13.39	24.01	2.40	20.77	-15.01	<0.01
			CV(%)	20.87	2.82	200.00	2.22	20.14	n/a
	0	0.51	mean	12.35	32.81	12.40	60.05	34.74	1.00
			CV(%)	0.65	1.10	0.61	6.73	13.79	0.00
		0.26	mean	5.42	65.92	5.25	323.05	290.20	1.00
			CV(%)	3.57	2.09	3.72	4.79	5.91	0.00

Table A-4. Friction parameter identification results of hyperbolic model for joint 2.

Joint	Extra load (N)	Maximum velocity (rad/s)	Statistic	Six-parameter hyperbolic model					
				γ_1	γ_2	γ_3	γ_4	γ_5	γ_6
2	33.1	1.01	mean	14.41	1015.80	16.29	16.49	15.54	23.63
			CV(%)	2.39	77.99	37.37	3.12	29.58	5.12
		0.51	mean	14.51	231.73	3.11	1.04	17.76	60.90
			CV(%)	2.96	3.60	5.35	157.19	104.80	4.56
		0.26	mean	86.93	51.73	12.50	0.21	9.85	99.37
			CV(%)	170.60	25.87	48.55	112.83	77.80	0.89
	0	1.01	mean	15.50	825.62	8.85	16.12	9.23	21.62
			CV(%)	6.13	69.49	49.46	29.84	36.66	17.12
		0.51	mean	14.26	224.90	2.62	<0.01	95.36	54.58
			CV(%)	0.28	2.62	1.85	n/a	116.70	0.90
		0.26	mean	12.37	59.79	8.67	0.01	7.18	89.69
			CV(%)	1.25	3.30	1.59	89.81	88.63	1.46

Table A-5. Friction parameter identification results of Coulomb plus viscous and Stribeck model for joint 3.

Joint	Extra load (N)	Maximum velocity (rad/s)	Statistic	Coulomb + viscous model		Four-parameter Stribeck model			
				c	v	F_k	F_v	F_s	V_c
3	33.1	2.03	mean	9.18	7.35	9.18	7.35	<0.01	1.00
			CV(%)	0.90	4.49	0.90	4.49	n/a	0.00
		0.51	mean	10.04	11.19	10.05	16.60	6.81	1.00
			CV(%)	1.76	6.15	1.74	15.78	48.00	0.00
		0.27	mean	6.90	21.94	6.90	21.94	<0.01	1.00
			CV(%)	2.72	3.13	2.72	3.13	n/a	0.11
	0	2.03	mean	8.34	5.20	8.34	5.20	<0.01	1.00
			CV(%)	1.58	8.53	1.58	8.53	n/a	0.00
		0.51	mean	10.16	9.62	10.16	9.62	<0.01	1.00
			CV(%)	2.76	9.34	2.76	9.35	n/a	0.10
		0.25	mean	7.26	24.31	7.26	24.31	<0.01	1.00
			CV(%)	2.46	7.23	2.46	7.23	n/a	0.00

Table A-6. Friction parameter identification results of hyperbolic model for joint 3.

Joint	Extra load (N)	Maximum velocity (rad/s)	Statistic	Six-parameter hyperbolic model					
				γ_1	γ_2	γ_3	γ_4	γ_5	γ_6
		2.03	mean	10.98	54.95	5.94	12.96	3.88	4.80
			CV(%)	1.30	6.54	1.93	2.50	3.62	4.97
	33.1	0.51	mean	8.16	1459.60	33.59	10.31	48.74	10.97
			CV(%)	3.15	19.98	4.81	2.17	3.71	5.95
		0.27	mean	9.26	148.54	5.15	2.37	10.27	36.95
3			CV(%)	2.80	2.36	4.10	8.93	6.35	1.86
		2.03	mean	10.22	53.01	6.06	11.27	4.16	3.24
			CV(%)	1.37	4.30	3.27	3.27	3.37	10.10
	0	0.51	mean	8.61	1177.70	41.29	10.58	52.83	9.06
			CV(%)	2.47	4.66	4.54	3.23	3.36	8.80
		0.25	mean	9.80	140.90	5.62	3.25	11.53	38.35
			CV(%)	1.55	1.06	1.20	11.52	2.00	7.23

Table A-7. Friction parameter identification results of Coulomb plus viscous and Stribeck model for joint 4.

Joint	Extra load (N)	Maximum velocity (rad/s)	Statistic	Coulomb + viscous model		Four-parameter Stribeck model			
				c	v	F_k	F_v	F_s	V_c
		2.00	mean	1.37	0.12	<0.01	0.06	-1.50	<0.01
			CV(%)	1.16	17.80	n/a	32.22	1.12	n/a
	33.1	1.51	mean	1.47	0.32	<0.01	0.30	-1.50	<0.01
			CV(%)	1.25	31.59	n/a	32.96	1.30	n/a
		0.81	mean	1.62	1.31	0.01	1.03	-1.86	0.01
4			CV(%)	3.99	11.88	200.00	17.09	4.45	14.49
		2.00	mean	1.51	0.36	<0.01	0.29	-1.66	0.01
			CV(%)	1.23	2.51	n/a	3.96	0.14	30.51
	0	1.51	mean	1.55	0.61	<0.01	0.57	-1.63	<0.01
			CV(%)	5.33	16.43	n/a	19.14	1.85	n/a
		0.79	mean	1.50	2.37	<0.01	1.90	-1.93	0.01
			CV(%)	12.68	22.15	n/a	32.74	14.10	26.52

Table A-8. Friction parameter identification results of hyperbolic model for joint 4.

Joint	Extra load (N)	Maximum velocity (rad/s)	Statistic	Six-parameter hyperbolic model					
				γ_1	γ_2	γ_3	γ_4	γ_5	γ_6
		2.00	mean	30.97	118.96	111.57	1.50	61.41	0.06
			CV(%)	5.77	11.73	11.39	1.15	10.36	31.63
	33.1	1.51	mean	1.79	208.84	20.71	1.54	16.45	0.27
			CV(%)	8.77	11.15	50.20	2.94	50.25	31.29
		0.81	mean	38.73	49.75	34.09	1.92	20.21	0.96
4			CV(%)	78.29	34.91	12.84	5.22	8.95	20.35
		2.00	mean	41.32	78.31	73.47	1.68	38.09	0.29
			CV(%)	37.47	21.08	19.14	0.37	12.40	3.64
	0	1.51	mean	1.67	553.90	8.45	1.81	6.75	0.43
			CV(%)	1.65	33.17	40.67	7.25	38.86	28.96
		0.79	mean	25.49	103.93	22.12	1.82	13.86	2.01
			CV(%)	116.70	45.04	99.31	42.79	61.67	61.57

Table A-9. Friction parameter identification results of Coulomb plus viscous and Stribeck model for joint 6.

Joint	Extra load (N)	Maximum velocity (rad/s)	Statistic	Coulomb + viscous model		Four-parameter Stribeck model			
				c	v	F_k	F_v	F_s	V_c
6	33.1	2.01	mean	1.18	0.30	<0.01	0.25	-1.30	0.01
			CV(%)	0.85	2.69	n/a	3.74	1.10	5.94
		1.51	mean	1.13	0.42	<0.01	0.36	-1.24	<0.01
			CV(%)	1.25	9.04	n/a	9.89	1.24	n/a
		0.80	mean	1.07	0.82	<0.01	0.55	-1.32	0.01
			CV(%)	4.27	11.14	n/a	19.19	4.31	7.35
	0	2.00	mean	1.20	0.30	<0.01	0.26	-1.30	0.01
			CV(%)	0.92	2.58	n/a	3.32	1.35	6.22
		1.50	mean	1.14	0.42	0.04	0.38	-1.18	<0.01
			CV(%)	2.86	8.66	200.00	7.38	6.80	n/a
		0.80	mean	1.05	1.02	0.19	1.20	-0.49	0.20
			CV(%)	7.18	28.71	200.00	95.42	332.60	195.10

Table A-10. Friction parameter identification results of hyperbolic model for joint 6.

Joint	Extra load (N)	Maximum velocity (rad/s)	Statistic	Six-parameter hyperbolic model					
				γ_1	γ_2	γ_3	γ_4	γ_5	γ_6
6	33.1	2.01	mean	1.55	75.54	11.45	1.21	11.56	0.30
			CV(%)	2.27	6.68	13.85	1.54	13.13	6.09
		1.51	mean	1.35	428.76	23.91	1.23	24.38	0.37
			CV(%)	2.93	18.07	34.97	3.08	38.30	3.30
		0.80	mean	20.06	62.45	58.12	1.30	41.43	0.57
			CV(%)	20.29	6.72	6.31	4.76	17.15	19.52
	0	2.00	mean	1.42	118.81	10.94	1.23	11.31	0.30
			CV(%)	1.20	5.81	13.81	1.14	13.86	3.17
		1.50	mean	1.25	687.14	22.64	1.24	23.95	0.36
			CV(%)	2.30	32.53	56.82	3.99	62.04	7.00
		0.80	mean	13.50	100.24	66.39	1.03	52.86	1.06
			CV(%)	48.94	22.58	48.62	50.04	50.13	77.03

APPENDIX B
ROOT MEAN SQUARE ERROR OF THREE FRICTION MODELS

Table B-1. Root mean square error of three different friction models for joint 1 and joint 2.

Joint	Extra load (N)	Maximum velocity (rad/s)	RMS error	Coulomb + viscous model	Stribeck model	Hyperbolic model
1	33.1	1.00	mean(Nm)	1.72	1.28	1.24
			CV(%)	5.00	5.16	5.47
			percentage(%)	6.39	4.75	4.62
		0.50	mean(Nm)	1.86	1.45	1.38
			CV(%)	1.37	2.33	2.45
			percentage(%)	9.04	7.02	6.71
		0.34	mean(Nm)	1.92	1.56	1.46
			CV(%)	1.32	4.56	1.83
			percentage(%)	10.49	8.52	7.96
	0	1.00	mean(Nm)	1.77	1.33	1.30
			CV(%)	4.20	4.02	4.17
			percentage(%)	6.59	4.93	4.82
		0.50	mean(Nm)	1.87	1.49	1.44
			CV(%)	1.87	1.76	1.96
			percentage(%)	9.01	7.21	6.94
		0.34	mean(Nm)	2.27	1.82	1.73
			CV(%)	9.79	8.77	8.68
			percentage(%)	10.78	8.61	8.22
2	33.1	1.01	mean(Nm)	3.73	2.57	2.57
			CV(%)	15.97	8.15	4.67
			percentage(%)	2.88	1.99	1.99
		0.51	mean(Nm)	3.01	2.99	2.37
			CV(%)	3.52	3.56	3.84
			percentage(%)	3.59	3.58	2.83
		0.26	mean(Nm)	3.11	3.02	2.79
			CV(%)	6.76	5.56	9.91
			percentage(%)	5.95	5.79	5.34
	0	1.01	mean(Nm)	3.70	2.43	2.46
			CV(%)	12.57	5.02	8.55
			percentage(%)	3.56	2.34	2.36
		0.51	mean(Nm)	2.93	2.92	2.28
			CV(%)	1.40	1.36	0.39
			percentage(%)	4.29	4.28	3.34
		0.26	mean(Nm)	2.86	2.82	2.51
			CV(%)	2.06	2.05	2.04
			percentage(%)	6.53	6.44	5.73

Table B-2. Root mean square error of three different friction models for joint 3 and joint 6.

Joint	Extra load (N)	Maximum velocity (rad/s)	RMS error	Coulomb + viscous model	Stribeck model	Hyperbolic model
3	33.1	2.03	mean(Nm)	3.10	3.10	2.67
			CV(%)	3.04	3.04	3.32
			percentage(%)	3.25	3.25	2.80
		0.51	mean(Nm)	1.30	1.30	1.11
			CV(%)	1.83	1.84	2.79
			percentage(%)	2.77	2.77	2.35
		0.27	mean(Nm)	2.03	2.03	1.68
			CV(%)	2.78	2.78	2.83
			percentage(%)	7.71	7.71	6.37
	0	2.03	mean(Nm)	2.51	2.51	2.08
			CV(%)	5.40	5.40	6.91
			percentage(%)	3.96	3.96	3.27
		0.51	mean(Nm)	1.12	1.12	0.97
			CV(%)	4.52	4.52	6.09
			percentage(%)	3.23	3.23	2.80
		0.25	mean(Nm)	2.24	2.24	1.84
			CV(%)	0.95	0.95	1.31
			percentage(%)	9.77	9.77	8.02
6	33.1	2.01	mean(Nm)	0.25	0.20	0.19
			CV(%)	4.10	3.74	3.89
			percentage(%)	6.45	5.09	4.88
		1.51	mean(Nm)	0.16	0.12	0.12
			CV(%)	7.76	12.05	12.04
			percentage(%)	4.66	3.47	3.38
		0.80	mean(Nm)	0.18	0.13	0.12
			CV(%)	4.28	10.97	11.58
			percentage(%)	6.41	4.57	4.43
	0	2.00	mean(Nm)	0.21	0.17	0.16
			CV(%)	3.82	3.07	3.22
			percentage(%)	5.38	4.31	4.19
		1.50	mean(Nm)	0.14	0.11	0.11
			CV(%)	17.75	18.18	18.06
			percentage(%)	4.10	3.17	3.12
		0.80	mean(Nm)	0.20	0.16	0.15
			CV(%)	30.14	49.17	47.23
			percentage(%)	6.49	5.20	4.97

LIST OF REFERENCES

1. P. Khosla and T. Kanade, “Parameter Identification of Robot Dynamics,” in *Proc. of 24th IEEE Conference on Decision and Control*, pp. 1754-1760, 1985.

2. C. T. Johnson and R. D. Lorenz, “Experimental identification of friction and its compensation in precise, position controlled mechanisms,” *IEEE Trans. Ind. Applicat.,* vol. 28, pp. 1392–1398, Nov./Dec. 1992.

3. B. Armstrong-Helouvry, *Control of machines with friction*, Kluwer Academic Publishers, 1991.

4. T.D. Tuttle, “Understanding and modeling the behavior of a harmonic drive gear transmission,” Master’s Thesis, MIT Artificial Intelligence Laboratory, 1992.

5. H.D. Taghirad, “On the modeling and identification of harmonic drive systems,” Centre for Intelligent Machines, McGill University. Tech. Rep. CIM-TR-97-02, 1997.

6. C. Canudas de Wit, H. Olsson, K. J. Astrom, and P. Lischinsky, “A New Model for Control of Systems with Friction,” *IEEE Transactions Automatic Control,* vol. 40, pp. 419-425, Mar. 1995.

7. J. Swevers, F. Al-Bender, C. G. Ganseman, and T. Prajogo, “An Integrated Friction Model Structure with Improved Presliding Behavior for Accurate Friction Compensation,” *IEEE Transactions Automatic Control,* vol. 45, pp. 675-686, Apr. 2000.

8. C. Makkar, W. E. Dixon, W. G. Sawyer, and G. Hu, “A new continuously differentiable friction model for control systems design,” in *Proc. IEEE/ASME Int. Conf. Adv. Intell. Mechatronics*, Monterey, CA, 2005, pp. 600–605.

9. C. W. Kennedy and J. P. Desai, “Estimation and modeling of the harmonic drive transmission in the Mitsubishi PA-10 robot arm,” in *Proc. IEEE/RSJ Int. Conf. Intell. Robots Syst.,* 2003, pp. 3331–3336.

10. N. Bompos, P. Artemiadis, A. Oikonomopoulos, and K. Kyriakopoulos, “Modeling, full identification and control of the Mitsubishi PA-10 robot arm,” in *Advanced intelligent mechatronics, 2007 IEEE/ASME international conference on,* September 2007, pp. 1–6.

11. C. Lightcap and S. A. Banks, “Dynamic identification of a Mitsubishi PA10-6CE robot using motion capture,” in *Proc. IEEE/RSJ Int. Conf. Intell. Robot. Syst*., San Diego, CA, 2007, pp. 3860–3865.

12. J. Swevers, J. Ganseman, and H. Van Brussel, “Experimental robot identification using optimized periodic trajectories,” *Mechanical Systems and Signal Processing*, vol. 10, no. 5, pp. 561-577, 1996.

13. G. Calafiore, M. Indri, and B. Bona, “Robot dynamic calibration: optimal excitation trajectories and experimental parameter estimation”, *Journal of Robotic Systems*, vol. 18, no. 2, pp. 55–68, 2001.

14. M. Spong, “Modeling and control of elastic joint robots,” *Journal of Dyn. Syst., Meas. and Cont.,* vol. 109, pp. 310-319, 1987.

15. K. Halvorsen, “Bias compensated least squares estimate of the center of rotation,” *Journal of Biomechanics*, vol. 36, pp. 999–1008, 2003.

16. C. Lightcap, S. Hamner, T. Schmitz, and S. Banks, “Improved positioning accuracy of the PA10-6CE robot with geometric and flexibility calibration,” *IEEE Trans. on Robotics*, submitted for publication, Jan. 2007.

17. W.E. Dixon, E. Zergeroglu, D.M. Dawson, and M.W. Hannan, "Global adaptive partial state feedback tracking control of rigid-link flexible-joint robots*", Robotica*, vol. 18, no. 3, pp. 325–336, 2000.

BIOGRAPHICAL SKETCH

Cheng Chen received a Bachelor of Science degree in Mechanical Engineering from Shanghai Jiaotong University, China. Then he entered University of Florida with research interest about dynamics and control. He decided to pursue his Master of Science degree at UF under the direction of Dr. Banks.